Analyst

# RAPID BLADDER CANCER CELL DETECTION FROM CLINICAL URINE SAMPLES USING AN ULTRA-THIN SILICONE MEMBRANE



| | |
|---|---|
| Journal: | *Analyst* |
| Manuscript ID | AN-ART-08-2015-001616.R1 |
| Article Type: | Paper |
| Date Submitted by the Author: | 22-Oct-2015 |
| Complete List of Authors: | Appel, Jennie; Arizona State University, Electrical Computer and Energy Engineering<br>Ren, Hao; Arizona State University, Electrical Computer and Energy Engineering<br>Sin, Mandy L. Y.; Stanford University, Urology<br>Liao, Joseph; Stanford University,<br>Chae, Junseok; Arizona State University, School of Electrical, Computer, and Energy Engineering |
| | |

# RAPID BLADDER CANCER CELL DETECTION FROM CLINICAL URINE SAMPLES USING AN ULTRA-THIN SILICONE MEMBRANE

*Jennie Appel[1], Hao Ren[1], Mandy L.Y. Sin[2], Joseph C. Liao[2], Junseok Chae[1]*

[1]School of Electrical, Computer and Energy Engineering, Arizona State University, USA

[2]Department of Urology, Stanford University School of Medicine, Stanford, USA

## Abstract

Early detection of initial onset, as well as recurrence, of cancer is paramount for improved patient prognosis and human health. Cancer screening is enhanced by rapid differentiation of cancerous from non-cancerous cells which employs the inherent differences in biophysical properties. Our preliminary testing demonstrates that cell-line derived bladder cancer cells deform our <30 nm silicone membrane within an hour and induce visually distinct wrinkle patterns while, cell-line derived non-cancerous cells fail to induce these wrinkle patterns. Herein, we report a platform for the rapid detection of cancerous cells from human clinical urine samples. We performed a blinded study with cells extracted from the urine of human patients presenting cancer-like symptoms alongside healthy controls. Wrinkle patterns were induced specifically by the five cancer patient samples within 12 hours and not by the healthy controls. These results were independently validated by the standard diagnostic techniques cystoscopy and cytology. Thus, our ultra-thin membrane approach for cancer diagnosis appears as accurate as standard diagnostic methods while vastly more rapid, less invasive, and requiring limited expertise.

**Keywords:** bladder cancer, cellular adhesion, biosensor, ultra-thin membrane

## Introduction

Bladder cancer is the fifth most common cancer in the United States with estimated 74,000 new cases in 2015 [1]. Since bladder cancer has a high rate of new tumor formation, a recurrence rate of up to 70%, lifelong surveillance is necessary as often as every 3 months which incurs significant expense and time commitment [2]. Current bladder cancer diagnosis is based on an invasive endoscopy procedure called cystoscopy followed by biopsy of suspect lesions for histological examination. To compensate for cystoscopy which lacks sensitivity for flat carcinoma [2] urine cytology—the microscopic examination of naturally exfoliated and expelled urothelial cells in the urine—is widely employed alongside cystoscopy. While highly specific (>95%), urine cytology has low (~20%) and moderate (~60%) sensitivity for low and high grade cancers, respectively [3]. As a consequence of this low sensitivity for early cancer detection, there are strong interests to develop urine-based diagnostics to complement and overcome shortcomings of cytology and cystoscopy. The majority of efforts have focused on developing molecular diagnostics based on cancer-associated genetic changes, as well as alterations in RNA and protein expression [4]. While several molecular assays are commercially available, significant shortcomings remain, which include diagnostic sensitivity and excessive cost, precluding widespread adaptation [4].

Quantitative measurement of cellular biophysical properties of cancerous and non-cancerous cells represents a promising alternative strategy for cancer diagnosis, given the intrinsic difference in size, cytoskeleton flexibility, morphology and stiffness of cancerous from non-cancerous cells. Many studies have investigated using microfluidics to isolate cancerous cells from blood cells based on the relative differences in cell size [5]. For example Li *et al*. used a combination of microfluidics and acoustic waveforms to effectively isolate more than 83% of cancerous cells from white blood cells [6]. Although this is highly effective for separating cells based on size, when the cell sizes are similar this method becomes less efficient, particularly for urine based samples. Young's modulus, a measurement of cellular stiffness, is particularly promising for cancerous cell detection when size based means are impractical [7-8]. For bladder cancer, Lekka *et al*. determined that cancerous cell lines HU456, T24, and BC3726 had an average Young's modulus of 0.8 kPa compared with 10.0 kPa for non-cancerous cell lines HU609 and HCU29 [7]. For oral cancer, cells extracted from patients with oral squamous cell carcinoma were three-fold more flexible than non-cancerous cells from healthy donors [8]. Tan *et al.* also compared the translocation time, related to cytoskeleton flexibility of T24, cell-line derived human bladder cancer cells, and immortalized non-cancerous human urothelial cells. These cell types were passed through a micro pore via an applied electric field. The non-cancerous urothelial cells had an order of magnitude increase in translocation time when compared to their cancerous counterparts [9]. Thus scanning force microscopy, optical stretching and translocation via applied electric field have all shown significant differences in the biophysical properties of cancerous and non-cancerous cells. The differences in Young's modulus and cytoskeleton flexibility between cancerous and non-cancerous cells are in part due to another biophysical property, the cellular traction forces applied to an *in vitro* surface. Cell traction forces can be visualized using micro-pillar structures [10] or silicone membranes [11-12]. Li *et al*. employed a silicon nano-pillar structure to determine that cancerous human Hela cells exerted 20% greater cell traction force when compared to non-cancerous fibroblasts harvested from neonatal rat liver [13]. The application of micro-pillars as a diagnostic device requires highly-optimized fabrication techniques and sophisticated analytical methodologies. Although these methods all show distinct differences between the biophysical properties of cancerous and non-cancerous cells, they have not been employed for cancer cell detection.

Here we report a high-throughput, based on the concurrent analysis of all cells present in the sample, strategy capable of differentiating bladder cancer cells from non-cancerous cells based on their respective cellular traction forces. Our method requires minimal sample preparation, does not demand highly-trained personnel for data interpretation, and only involves an inexpensive low-power microscope. Our approach leverages an ultra-thin, <30 nm, silicone membrane to visualize the distinct cell traction forces of bladder cancer cells. Our ultra-thin silicone membrane is deformed exclusively by cancerous cells, producing distinct wrinkle patterns compared to non-cancerous cells [14]. In this study, we examined the underlying mechanism for ultra-thin membrane deformation exclusively by cancerous bladder cells by manipulation and visualization of focal adhesion proteins. Furthermore, clinical validation of our cancer detection strategy was performed. A blinded study was performed using urine collected from five individuals presenting cancer-like symptoms. And within 12 hours, of sample collection cancer cells present in all five patient urine samples generated wrinkle patterns. Our technique circumvents traditionally complex, costly, and invasive instrumentation for bladder cancer screening and detection as well as may be applied for the detection of additional cancers.

## Results and Discussion

Ultra-thin Membrane Characterization

Previous reports have focused on the visualization of cell locomotion with cancerous cells on uncharacterized silicone membranes of various thicknesses [11-12] and characterized using calibrated microneedles [15]. Dembo *et al*. performed a thorough investigation into the material properties of the membrane formed by flash-heating liquid silicone. They performed a "pinch" test which compressed the membrane and allowed for the calculation of Young's modulus which they determined to be 54±15 dyn/cm [15]. We characterized our silicone membrane by applying a minute droplet of water to the surface [14, 16]. The approximately 0.5 μL of water on the surface of membrane induced a radial wrinkle pattern (supplementary figure 1(b)). From the wrinkle pattern, the thickness of the membrane was calculated to be approximately 28 nm. A predictive estimation of the wavelength, amplitude and number of wrinkles is included in the supplemental materials [17].

Wrinkle Pattern from Cell-line Derived Cancerous Cells

We compared the time and extent of membrane wrinkle formation generated by cell-line derived low grade bladder papillary carcinoma RT4 cells, used as a control (figure 1 (a)). In this study, we evaluated and compared RT4 cells to a cell-line derived high grade bladder carcinoma T24 cells. Cancer grades represent tumor severity and the likelihood of metastasis within human patients. Approximately $5x10^5$ RT4 or T24 cells were applied to our silicone membrane, and distinct wrinkles were generated by both within blank hours (figure 1 (a) & (b)). To elucidate the onset of wrinkle pattern formation for cancerous RT4 and T24 cells, a time-lapse experiment was performed for 4-, 6-, and 8-hour incubation periods; as opposed to a time-lapse experiment using only RT4 cells at 18-, 20-, and 22-hour incubation periods. Both the RT4 cells (supplementary figure 2 (a)-(d)) and the T24 cells (supplementary figure 2 (e)-(h)) induced wrinkle patterns after 4 hours of incubation. Additionally experimental set-up is shown in supplementary figure 2. By examining the aggregate number of wrinkle patterns generated at various time intervals, we found a positive correlation between the number of wrinkles patterns and the time of incubation (figure 1 (c)). In contrast, the number of individual wrinkles and the length of these wrinkles, which comprise individual wrinkle patterns, showed little direct correlation with the incubation time (figure 1 (d)). For example, RT4 cells generated on average 5.7 individual wrinkles after 8 hours, while T24 cells generate 2.3 individual wrinkles. It is also interesting to note that typically if only one cell generates a wrinkle pattern then the number of wrinkles ranges from 1 to 3. However if multiple cells are clustered together then the number of induced wrinkles typically increases beyond 3. However if the cells are not clustered together then the wrinkle patterns generated by each individual cell are not impacted by the presence of non-wrinkle generating cells or other cells which do generate wrinkle patterns. Our representative cancerous cells generated wrinkle patterns as early as four hours and the wrinkle patterns formed persisted over the entire length of observation.

To ensure that selectively cancerous cells induce wrinkle pattern formation on our ultra-thin silicone membrane, we used a non-cancerous healthy control of cell-line human kidney epithelial (HEK293f) cells. HEK293f cells were chosen due to the high degree of similarity between the epithelial cells found in the kidney and the bladder cavity. Approximately $5x10^5$ HEK293f cells were applied to our membrane. HEK293f cells failed to generate discernable

wrinkle patterns or individual wrinkles (supplementary figure 2 (i)-(l)) after extended incubation period of 24 hours. Thus cell-induced wrinkle pattern formation was specific to the cancerous cell-line derived cells we tested and not shared with non-cancerous cell-line derived cells.

To better replicate potential clinical testing of human patient samples, we placed cell-line derived cancerous cells in modified urine environments. This simulates the conditions in which cells could not be readily extracted from human urine by centrifugation and instead whole urine samples would be applied to the membrane, such as in developing nations. We incubated cancerous RT4 or T24 cells on ultra-thin membranes in human (figure 2 (b)) or artificial (figure 2 (a)) urine at pH varying from 5 to 7, within the typical range of human urine [18]. To sustain the cancerous cell-line derived RT4 or T24 cells for extended device testing, we supplemented the clarified—by centrifugation—human or artificial urine with 10 % fetal bovine serum. As expected, the cancerous RT4 and T24 cells retained the ability to induce membrane deformation and generated wrinkle patterns in both human and artificial urine, across all tested pH values. The number of wrinkle patterns was not a function of the type of urine, human or artificial, or the pH value (figure 2). Thus the inherent biophysical properties differences responsible for cancer-specific wrinkle formation is not affected by the urine or changes in pH.

Wrinkle Patterns from a Mixture of Cancerous and Non-cancerous Cells

First we examined the capacity of cancerous RT4 cells to generate wrinkle patterns in the presence of non-cancerous cells HEK293f and buffy coat cells. Buffy coat is the fraction of blood that is comprised principally of white blood cells. White blood cells are often found in clinical patient urine, as one of the primary symptoms of bladder cancer is hematuria or blood within the urine. We examined the attributes of the present wrinkle patterns, i.e. number and length of wrinkles within each wrinkle pattern. Quantitation of the number of wrinkles within a wrinkle pattern was performed by serially counting the number of wrinkles generated by each cluster of cancerous cells or an individual cancerous cell. The length of each wrinkle within a wrinkle pattern was measured relative to the diameter of a cell, approximated as 20 μm. No apparent correlation was observed between mixture ratio and these wrinkle pattern attributes. However, a strong inverse trend was found between the overall number of wrinkle patterns and mixture ratio (figure 3 (a) & (b)). Wrinkle patterns are defined as the culmination of wrinkles generated by a cluster or individual cell within a discrete span separate from other cells and induced membrane deformations of the ultra-thin membrane. Therefore by examining the overall number of wrinkle patterns we can better represent clinical use of the ultra-thin membrane diagnosis platform, because a clinician would only need to determine if wrinkle patterns are present. Clinical patient urine samples are composed of a very small population of cancerous cells in the presence of an overwhelmingly non-cancerous cell population. Therefore increasing the number of non-cancerous cells better simulates clinical samples. Additional experimentation by varying mixture ratios to deplete the population of cancerous cells is necessary to define a true threshold for detection. However, in clinical applications approximations of the actual number of cancer cells present in a urine sample could be determined based on the number of wrinkle patterns present.

Clinical Urine Sample Testing

To validate the ultra-thin membrane as a detection tool of human patient bladder cancer, we obtained urine samples from five individuals presenting cancer-like symptoms. All patients

were male ages 53 to 89. And four of the five patients were being treated for a recurrence of bladder cancer. Additionally, two of the five patients reported a history of smoking. Urine samples were collected during a transurethral resection of bladder tumor (TURBT) procedure, which is the standard method for endoscopic resection and local staging of bladder cancer [19]. Also a control urine sample was collected from a female healthy donor without family history of bladder cancer. Cells were extracted from all urine samples, washed and applied to the ultra-thin membrane.

Following 12 hours of incubation, wrinkle patterns were observed in the five bladder cancer patient samples (supplementary figure 3). Additionally, the healthy donor control cells failed to generate wrinkle patterns even after an extended incubation period of 24 hours (supplementary figure 2 (m)-(p)). The actual number of wrinkle patterns observed (table 1), ranging from 1 to 5, corresponds to less than a wrinkle pattern per ultra-thin membrane. This indicates that despite the low concentration of cancer cells, practical use of the ultra-thin membrane for cancer detection is well within the membrane detection limit which is dependent on the concentration of cancer cells in the urine sample.

TURBT provided pathological diagnosis of bladder cancer in the five patients. TURBT is performed by an endoscopic examination of the bladder interior and upon finding abnormal tissue extracting a small biopsy. This biopsy is then sent for examination by an experienced cytopathologist. As a complementary diagnosis method urine cytology is performed. This method is also dependent on an experienced cytopathologist to extract cells from urine and examine for abnormal cellular structure. For the purposes of this experiment patients had previously undergone either cytology, cystoscopy or both before TURBT (table 1). However, the patient prognosis was unknown until after analysis of the biopsy collected during TURBT. Interestingly, of the five patient samples, two—patient #2 and #3—demonstrated false negative results, i.e. negative for malignancy, by standard urine cytology, while generating an accurate positive result on our ultra-thin silicone membrane. Thus, initial validation of our ultra-thing silicone membrane demonstrates that this is a promising platform as thus far it is highly sensitive and accurate for the detection of human patient bladder cancer from urine samples.

Validation of Cell Traction Forces that Generate Wrinkle Patterns

To further characterize and identify the working mechanisms of wrinkle pattern formation, we varied the cell transfer method. T24 cells were removed from culture dishes by the addition of the protease trypsin or a cell dissociation buffer applied to our ultra-thin silicone membranes and imaged at 1 hour intervals for a total of four hours. This allows us to determine if the rate limiting step in wrinkle formation is due to properties of the ultra-thin membrane or properties of cancerous cells. While the T24 cells treated with the protease trypsin required three hours for initial wrinkle pattern formation, the T24 cells treated with the cell dissociation buffer generated wrinkles within a single hour (figure 4 (a)). The initial transfer method relied on trypsin which digests the focal adhesion proteins on the surface of the cell which must be regrown prior to cell-induced wrinkle formation. By shifting to a cell dissociation buffer, the focal adhesion proteins remain intact which dramatically reduces the time for wrinkle pattern formation, by negating regeneration of the adhesion protein. Therefore, we were able to decrease the time for cancerous cell wrinkle formation to one hour post cell addition to our membrane by changing the cell transfer method and determine that the rate limiting step in wrinkle formation is due to the properties of cancerous cells.

In an effort to make wrinkle patterns generated by RT4 cells more distinctive, we investigated a means of increasing the individual attributes of wrinkle patterns. We attempted to increase the individual number and length of wrinkles within a wrinkle pattern by coating the membrane with fibronectin, a cellular adhesion promoting protein. However, the average number and average length of wrinkles did not significantly vary with the addition of fibronectin (figure 4 (b)). Treatment of our ultra-thin silicone membrane surface with fibronectin failed to significantly affect the induction of membrane wrinkles measured by the number or length of individual wrinkles within wrinkle patterns.

To validate that cancerous cells are mechanically capable of generating sufficient strain, to induce deformation of our ultra-thin silicone membrane to produce wrinkle patterns. The observed strain induced deformation of our membrane by cancerous RT4 cells was compared to previously reported strain generated by cancerous cells [9]. Water droplet calibration of the membrane approximated 0.1% to 0.4% lumped strain (supplementary figure 1 (b)). This correlates well with lump strain we derived from a study of cell traction forces of on a polydimethylsiloxane micro-pillar structure, which was estimated to be 0.5% lump strain [9]. We derived this lump strain by averaging the strain generated by the displacement of each micro-pillar. This averaged strain was then normalized by the ratio between the surface area of each pillar in contact with the cell over the total area of the cell [9]. Additionally, a positive correlation between cellular traction force and metastatic potential of cancerous cells has been reported [20-21]. Thus the strain, as measured by cell traction forces, visualized by the number of wrinkles within a wrinkle pattern could be applied for discerning the grade of a cancer cell.

Cell traction forces are responsible for inducing strain in the ultra-thin membrane; these forces are dependent on focal adhesion proteins. Filamentous-actin (f-actin), a focal adhesion protein integral for cell shape, relocates to the edges of the cell for cell locomotion and spreading upon a surface [22]. Thus a focus of f-actin indicates that a force is being applied by the cell to an external surface [22]. To verify that the cytoskeleton of cancerous cells induces membrane deformation and generates wrinkle patterns in our ultra-thin silicone membrane, we fluorescently stained the f-actin with philotoxin. Philotoxin specifically binds to f-actin and the co-localization of philotoxin adjacent to wrinkle patterns would strongly support cellular adhesion being responsible for the membrane deformation. Following 24 hours of incubation of on the membrane, we fixed and stained T24 or HEK293f cells to visualize the localization of f-actin relative to wrinkle formation. Individual (figure 5 (a) – (c)) and clusters (figure 5 (d) – (f)) of T24 cells both generated two wrinkles, and more importantly the fluorescently stained f-actin co–localized with these wrinkles. Within an individual T24 cell, a locus of f-actin co-localized with the origins of wrinkles produced by the cell (figure 5 (c)). An intensity trace of fluorescence adjacent to the wrinkle showed a dramatic increase in fluorescence, and thus and increased presence f-actin at this location (supplementary figure 4 (a) & (c)). In contrast, individual and clusters of HEK293f cells failed to generate wrinkles (figure 5 (g) – (l)), did not have any discernable locus of f-actin, and the fluorescent intensity trace showed homogeneous intensity within the cell (supplementary figure 5 (b) & (d)). The co-localization of an f-actin locus immediately adjacent to the origin of the wrinkle patterns generated by cancerous T24 cells, along with the lack an f-actin locus in non-cancerous HEK293f cells, which fail to induce wrinkling, supports the cytoskeleton of cancerous cells inducing the deformation of the membrane and ultimately for wrinkle pattern formation. This indicates that the cytoskeleton of the T24 cell is exerting a force on the ultra-thin membrane which does induce wrinkle pattern

formation. Thus the underlying mechanism for membrane wrinkle formation appears dependent on f-actin foci and thus the cytoskeleton. While ancillary for clinical evaluation of patient samples, examining the underlying mechanism for wrinkle pattern formation gives insight into the inherent biophysical differences behind wrinkle pattern formation.

## Conclusion

Results from our blinded study on human patients with bladder cancer-like symptoms show that cells extracted from clinical urine samples can selectively deform our ultra-thin silicone membrane and generate wrinkle patterns. While cells extracted from the urine of healthy donors fail to sufficiently induce wrinkle formation. We confirm via manipulation and labeling of cellular adhesion proteins that this innate difference in the ability to generate wrinkle patterns in our membrane is in part due to the unique biophysical properties of cancerous cells from healthy counter parts. Thus, our ultra-thin silicone membrane has the potential to be developed into a simple, yet cost effective tool to discern the presence of bladder cancer from cells present in urine samples. Furthermore, our methodology can be applied toward the diagnosis of additional cancers where cells are easily obtained or naturally expelled, e.g. lung cancer detection through analysis of sputum. Moreover, our cancer diagnosis approach is highly amenable to developing nations where conventional diagnosis is cost-prohibitive and impedes continuous monitoring for initial onset and recurrences of cancer. Our device leverages inherent biophysical properties of cancerous cells for non-invasive, improved early detection and continuous surveillance for the recurrence of cancer.

## Materials and Methods

### Device Fabrication

Ultra-thin silicone membranes were formed by adding ~45μL of 12,500 cP viscosity liquid silicone (Brookfield Engineering Laboratories) to a 15 mm by 0.5 mm glass depression slide (Ted Pella, Inc.). The uppermost layer of silicone was cross-linked by inverting the slide over a flame for 5 to 10 seconds. The cell culture chamber was formed by attaching a 1.9 cm diameter by 2.54 cm height section of sterile PVC with vacuum grease to the glass slide (supplementary figure 1(a)) [14]. In some experiments, ultra-thin silicone membrane surfaces were modified by the addition of 10 μg fibronectin (BD Biosciences) in 1X PBS, incubated at room temperature for 1 hour, aspirated and membranes washed three times with 1X PBS.

### Cell Culture

RT4 is an established bladder cell-line derived from low grade human transitional cell papilloma. T24 is derived from high grade human transitional cell carcinoma. HEK293f is a transformed human embryonic kidney cell-line that served as non-cancerous controls to simulate epithelial cells found in non-cancerous urine samples. RT4 and T24 cells were grown in McCoy's 5A modified media (Life Technologies) and HEK293f cells were grown in Eagle's minimum essential medium (ATCC). Media was supplemented with 10% fetal bovine serum (FBS, Life Technologies), and 1X penicillin/streptomycin (Sigma-Aldrich). Cells were maintained in a 5% $CO_2$ environment at 37˚C.

### Cell-line Sample Preparation

Cells at 80% confluency were trypsinized (Invitrogen) or incubated with cell dissociation buffer (Life Technologies) for 5 min at 37˚C and washed with media supplemented with 10% FBS. Approximately $5x10^5$ cells were applied to each device and incubated in culture media with at 5% $CO_2$ at 37˚C. For simulating clinical samples with hematuria, $5x10^5$ white blood cells from buffy coat (Innovative Research) were applied to the ultra-thin membrane prior to applying RT4 or HEK293f. For urine pH effect, artificial urine (Spectrum Laboratories Inc.) or clarified aggregated donor urine samples were supplemented with 10% FBS and the pH adjusted with hydrochloric acid.

Patient and Healthy Donor Sample Preparation

With local institutional review board (IRB) approval, five urine samples were obtained from men ages 53 to 89 undergoing transurethral resection of bladder tumor (TURBT) [19] at VA Palo Alto Health Care System and a sixth urine sample was collected from a healthy female donor control with no family history of bladder cancer. Informed consent was obtained from all patients. Cells present in the urine were pelleted by centrifugation at 300 x gravity, washed twice with 1X PBS and re-suspended in McCoy's 5A modified media supplemented with 10% FBS prior to application to the ultra-thin silicone membrane.

Data Analysis

The pattern generated when a cluster or individual cell deforms the ultra-thin membrane is defined as a wrinkle pattern. Wrinkle patterns consist of a number of wrinkles which have various lengths. In addition, wrinkle patterns were quantified by measuring the number and length of each wrinkle following addition of cells to ultra-thin silicone membrane.

Fluorescent Imaging

F-actin was fluorescently labeled with Alexa Fluor 488 Phalloidin phallotoxin (Life Technologies) following the manufacturer's instructions. Briefly,T24 and HEK293f cells were pre-incubated on the ultra-thin silicone membrane for 24 hours were fixed with 4% paraformaldehyde in 1X PBS for 10 min at 37˚C, washed twice with 1X PBS, permeabilized with 0.1% Triton X-100 in 1X PBS for 10 min at 37˚C and washed twice with 1X PBS. The permeabilized cells were incubated with fluorescent Alexa Fluor 488 Phalloidin phallotoxin for 20 min at room temperature, washed twice with 1X PBS and visualized under a confocal microscope (Nikon Eclipse TE2000-U). Fluorescent intensity traces were measured using Image J and the data was binned for every 4 values.

## Acknowledgements

We would like to thank Dr. Julien Chen for HEK293f cell culture protocols, Dr. Joshua Podlevsky for his invaluable technical discussion and reading of the manuscript, Jorge Jimenez for his assistance with cell culture, and Dr. Kathy Mach for technical discussion. This work is supported by the NSF Graduate Research Fellowship under Grant No. DGE-1311230.

## References

[1] American Cancer Society. Cancer.org. 2015.

[2] S. Aldousari, and W. Kassouf, “Update on the management of non-muscle invasive bladder cancer” Can Urol Assoc J, 4(1): 56–64, Feb 2010.

[3] J. M. Tomasini and B. R. Konety, “Urinary Markers/Cytology What and When Should a Urologist Use” Urol Clin North Am. 40(2):165-73 May 2013.

[4] G. Cheung, A. Sahai, M. Billia, P. Dasgupta, and M. S. Khan, "Recent advances in the diagnosis and treatment of bladder cancer," BMC medicine, vol. 11, p. 13, 2013.

[5] Y. Chen, P. Li, P.H. Huang, Y. Xie, J. D. Mai, L. Wang, N.T. Nguyen, and T. J. Huang, “Rare cell isolation and analysis in microfluidics,” Lab on a Chip, vol. 14, pp. 626-645, 2014.

[6] P. Li, Z. Mao, Z. Peng, L. Zhou, Y. Chen, P.H. Huang, C. I. Truica, J. J. Drabick, W. S. El-Deiry, M. Dao, S. Suresh, and T. J. Huang, “Acoustic separation of circulating tumor cells,” PNAS, vol. 112, pp. 4970-4975, 2015.

[7] M. Lekka, P. Laidler, D. Gil, J. Lekki, Z. Stachura, and a. Z. Hrynkiewicz, "Elasticity of normal and cancerous human bladder cells studied by scanning force microscopy," European biophysics journal : EBJ, vol. 28, pp. 312-6, 1999.

[8] T.W. Remmerbach, et al. Cancer Research 69.5 (2009): 1728-32

[9] J. L. Tan, J. Tien, D. M. Pirone, D. S. Gray, K. Bhadriraju, and C. S. Chen, "Cells lying on a bed of microneedles: an approach to isolate mechanical force.," Proceedings of the National Academy of Sciences of the United States of America, vol. 100, pp. 1484-9, 2003.

[10] A. Ilyas, W. Asghar, S. Ahmed, Y. Lotan, J.-T. Hsieh,Y.-t. Kim and S. M. Iqbal, “Electrophysiological analysis of biopsy samples using elasticity as an inherent cell marker for cancer detection” Analytical Methods, 2014

[11] A. Harris, P. Wild, and D. Stopak, "Silicone Rubber Substrata: A New Wrinkle in the Study of Cell Locomotion” Science, vol. 208, pp. 177-179, 1980.

[12] R. J. Pelham and Y. L. Wang, "High resolution detection of mechanical forces exerted by locomoting fibroblasts on the substrate," Molecular biology of the cell, vol. 10, pp. 935-45, 1999.

[13] Z. Li, J. Song, G. Mantini, M.-Y. Lu, H. Fang, C. Falconi, L.-J. Chen, and Z. L. Wang, “Quantifying the Traction Force of a Single Cell by Aligned Silicon Nanowire Array” Nano Letters, vol. 9 issue 10 pp. 3575-3580, 2009

[14] J. Appel, M.L.Y. Sin, J.C. Liao, J. Chae, “Wrinkle Cellomics: Screening Bladder Cancer Cells using an Ultra-Thin Silicone Membrane,” Poster session presented at: IEEE 27th International Conference on Micro Electro Mechanical Systems (MEMS). 2014 Jan. 26-30. San Francisco, CA

[15] M. Dembo, T. Oliver, A. Ishihara, and K. Jacobson, “Imaging the Traction Stresses Exerted by Locomoting Cells with the Elastic Substratum Method” Biophysical Journal, Vol. 70, pp. 2008-2022, 1996.

[16] J. Huang, M. Juszkiewicz, W. H. de Jeu, E. Cerda, T. Emrick, N. Menon, et al., "Capillary wrinkling of floating thin polymer films.," Science, vol. 317, pp. 650-3, 2007.

[17] E. Cerda and L. Mahadevan, "Geometry and Physics of Wrinkling", Physical Review Letters, 90, 2003

[18] M. E. Wright, D. S. Michaud, P Pietinen, P. R. Taylor, J. Virtamo, D. Albanes, "Estimated urine pH and bladder cancer risk in a cohort of male smokers (Finland)." Cancer Causes and Control, vol. 16, issue 9, pp. 1117-23, Nov. 2005

[19] M. Babjuk, "Transurethral Resection of Non–muscle-invasive Bladder Cancer" European Urology Supplements, vol. 8, pp. 542–548, 2009

[20] M. Casey, Kraning-Rush, J. P. Califano, C. A. Reinhart-King, "Cellular Traction Stresses Increase with Increasing Metastatic Potential" PLoS ONE 7(2): e32572.

[21] T.M Koch, S. Münster, N. Bonakdar, J.P. Butler, B. Fabry (2012) "3D Traction Forces in Cancer Cell Invasion". PLoS ONE 7(3): e33476.

[22] D.-H. Kim, S. B. Khatau, Y. Feng, S. Walcott, S. X. Sun, G. D. Longmore, D. Wirtz, "Actin cap associated focal adhesions and their distinct role in cellular mechanosensing" Scientific Reports, vol. 2, article 555, 2012

**Figures**

**Figure 1:**

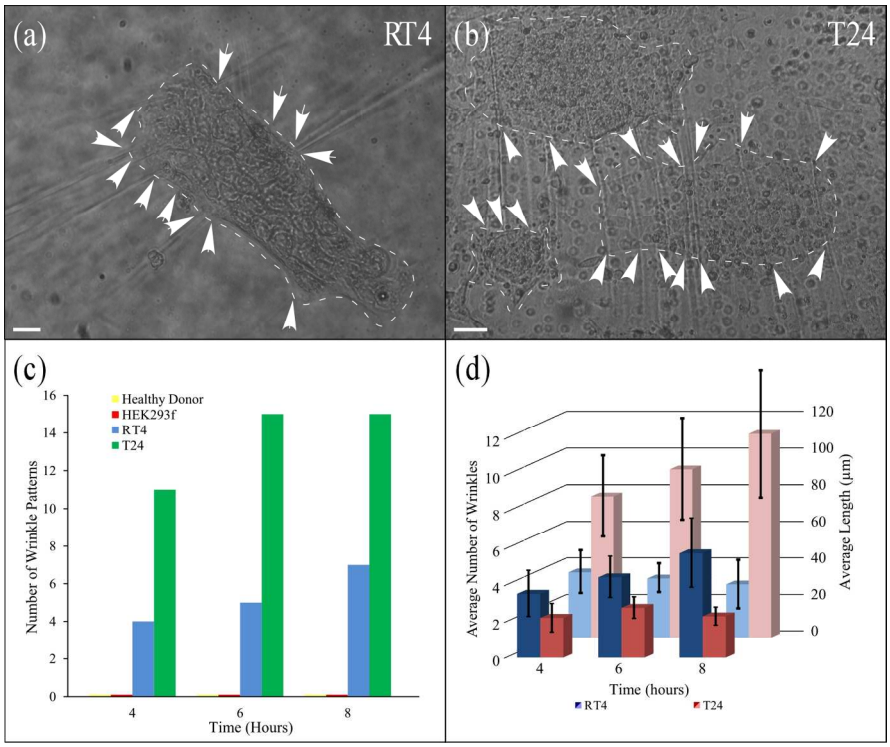

**Figure 2:**

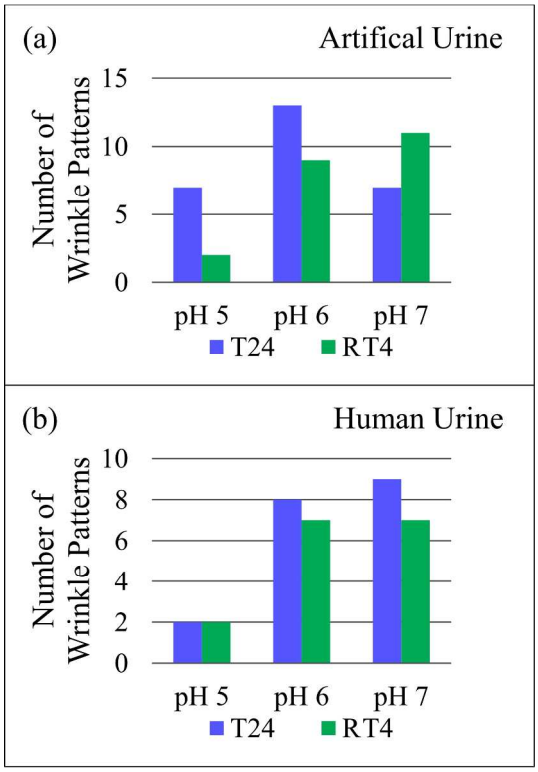


**Figure 3:**

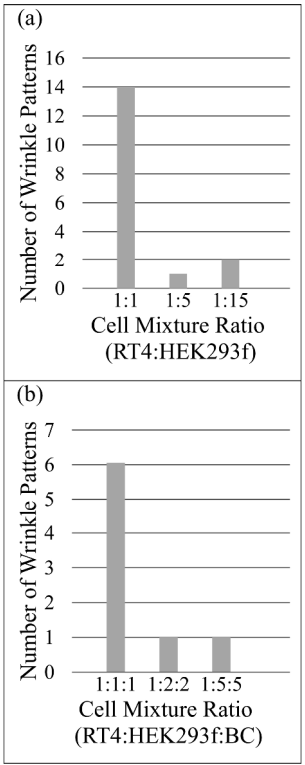

**Figure 4:**

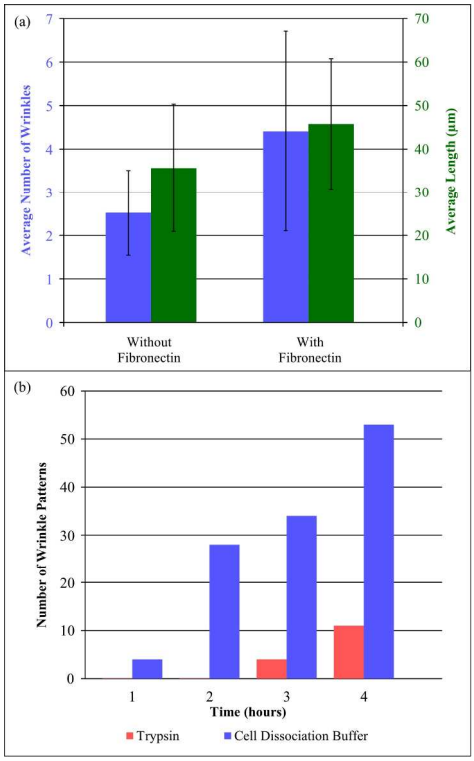


**Figure 5:**

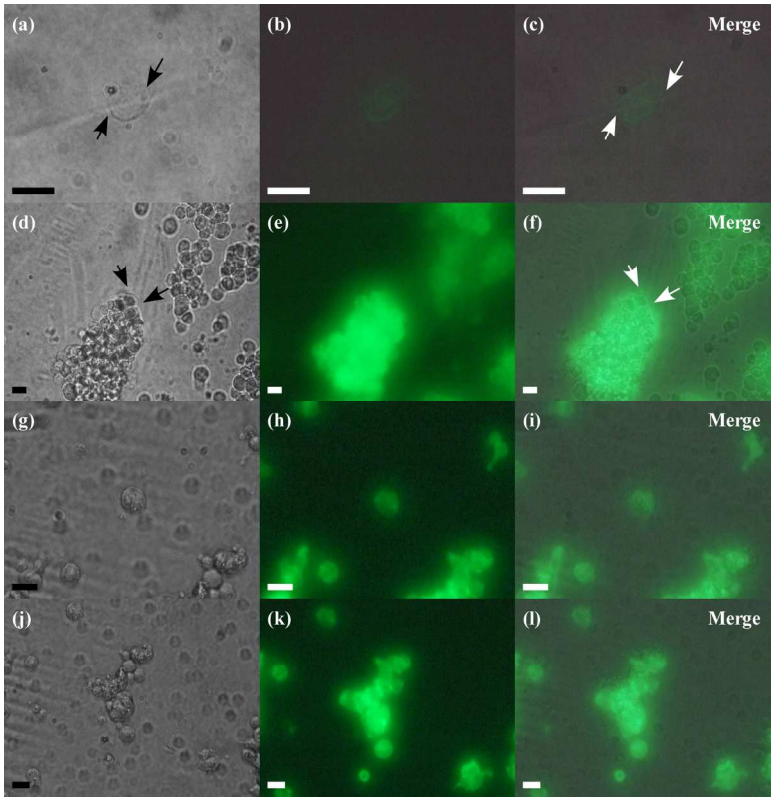


**Table 1:**

| Patient | Sex/ Age | Urine Collection Method | Cystoscopy | Cytology | Diagnosis | Wrinkle Patterns | Number of Wrinkle Patterns |
|---|---|---|---|---|---|---|---|
| 1 | M / 53 | TURBT | (10/23/2014) recurrence of bladder tumor at right UO, possibly involving distal right ureter | (10/23/2014) few atypical papillary-like structures are seen associated with bland appearing urothelial cells. The findings are atypical. | non-invasive papillary carcinoma low grade | Yes | 2 |
| 2 | M / 71 | TURBT | small papillary recurrence at bladder neck on recent surveillance cysto | (11/05/2014) Negative for malignancy | non-invasive papillary carcinoma low grade | Yes | 2 |
| 3 | M / 89 | TURBT | (11/6/2014) recurrent small bladder tumor near L UO | (11/05/2014) Negative for malignancy | non-invasive papillary urothelial carcinoma low grade | Yes | 1 |
| 4 | M / 80 | TURBT | Not Available | (11/6/2014) atypical, there are cells with hyperchromatic nuclei, irregular nuclear contour and prominent nucleoli. Differential diagnosis includes reactive changes and neoplasia. | non-invasive papillary urothelial carcinoma high grade | Yes | 1 |
| 5 | M / 67 | TURBT | Not Available | cytology (11/3/2014) suscipicious for malignancy (urothelial cells with enlarged nuclei, high N:C ratios and irregular nuclear contours.) | non-invasive papillary carcinoma high grade | Yes | 5 |
| 6 | F / 26 | Urination | Not Applicable | Not Applicable | No Cancer | No | NA |

## Figure Captions

Figure 1: Wrinkle Pattern Formation and Analysis (a) Approximately 75 RT4 cells generating a wrinkle pattern which consists of 12 wrinkles with an average length of 75 μm, after more than 24 hours. (b) Approximately 150 T24 cells generating 3 wrinkle patterns, the top pattern consists of 5 wrinkles with an average length of 50 μm, the middle pattern consists of 13 wrinkles with an

average length of 60 μm, and the bottom pattern consists of 3 wrinkles with an average length of 80 μm, after more than 24 hours. (c) Plot of the total number of wrinkle patterns generated by each cell type: RT4, T24, HEK293f, and Healthy Donor, at each time interval. (d) Plot showing the average attributes of a wrinkle pattern generated by either RT4 or T24 cells at each time interval. All scale bars are 20 μm.

Figure 2: Analysis of Wrinkle Patterns in Urine of Varying pH Levels (a) Plot of the number of wrinkle patterns generated by either RT4 or T24 cells in artificial urine at various pH levels. (b) Plot of the number of wrinkle patterns generated by either RT4 or T24 cells in a mix of purified healthy donor urine at various pH levels.

Figure 3: Wrinkle Patterns in Mixed Cell Populations (a)Plot of the number of wrinkle patterns generated by cancerous cells in each mixture ratio (RT4:HEK293f) (b) Plot of the number of wrinkle patterns generated by cancerous cells in each mixture ratio (RT4:HEK293f:buffy coat).

Figure 4: Comparing Cell Transfer Methods and Adhesion Promoting Proteins (a) Plot of the total number of wrinkle patterns generated over time after being transferred using either trypsin or a cell dissociation buffer. (b) Plot of the average attributes of a wrinkle pattern generated by RT4 cells after 12 hours in either unmodified devices or devices coated with fibronectin.

Figure 5: Fluorescent Staining of F-Actin in Cells Which Generate Wrinkle Patterns (a) A fixed individual T24 cell generating a wrinkle pattern consisting of 2 wrinkles with an average length of 40 μm. (b) Fluorescently stained F-actin in the T24 cell from (a). (c) Merge of (a) & (b) where both images are 60% opaque. (d) A fixed cluster of T24 cells generating a wrinkle pattern consisting of 2 wrinkles with an average length of 60 μm. (e) Fluorescently stained F-actin in the T24 cell cluster from (d). (f) Merge of (d) & (e) where both images are 60% opaque. (g) A fixed individual HEK293f cell. (h) Fluorescently stained F-actin in the HEK293f cell from (g). (i) Merge of (g) & (h) where both images are 60% opaque. (j) A fixed cluster of HEK293f cells. (k) Fluorescently stained F-actin in the cluster of HEK293f cells from (j). (l) Merge of (j) & (k) where both images are 60% opaque. All cells were fixed after more than 12 hours. All scale bars are 20 μm.

Table 1: Comparison of Clinical Patient Diagnosis Methods and Wrinkle Pattern Detection. Relevant patient information including sex, age, prior cystoscopy and cytology results as well as the observation of wrinkle pattern formation and the aggregate number of wrinkle patterns for each patient sample if applicable.